© 2017. Published by The Company of Biologists Ltd | Journal of Cell Science (2017) 130, 1404-1412 doi:10.1242/jcs.194662

RESEARCH ARTICLE

GSK3-mediated CLASP2 phosphorylation modulates kinetochore dynamics

Hayley Pemble*, Praveen Kumar‡, Jeffrey van Haren and Torsten Wittmann§

ABSTRACT

Error-free chromosome segregation requires dynamic control of microtubule attachment to kinetochores, but how kinetochore–microtubule interactions are spatially and temporally controlled during mitosis remains incompletely understood. In addition to the NDC80 microtubule-binding complex, other proteins with demonstrated microtubule-binding activities localize to kinetochores. One such protein is the cytoplasmic linker-associated protein 2 (CLASP2). Here, we show that global GSK3-mediated phosphorylation of the longest isoform, CLASP2α, largely abolishes CLASP2α–microtubule association in metaphase. However, it does not directly control localization of CLASP2α to kinetochores. Using dominant phosphorylation-site variants, we find that CLASP2α phosphorylation weakens kinetochore–microtubule interactions as evidenced by decreased tension between sister kinetochores. Expression of CLASP2α phosphorylation-site mutants also resulted in increased chromosome segregation defects, indicating that GSK3-mediated control of CLASP2α–microtubule interactions contributes to correct chromosome dynamics. Because of global inhibition of CLASP2α–microtubule interactions, we propose a model in which only kinetochore-bound CLASP2α is dephosphorylated, locally engaging its microtubule-binding activity.

KEY WORDS: CLASP2, GSK3, Kinetochore, Microtubule, Mitosis, Phosphorylation

INTRODUCTION

Kinetochores (KTs) are large protein complexes that connect mitotic chromosomes to spindle microtubules (MTs) and are essential for chromosome alignment and segregation. Despite enormous progress in revealing KT composition and structure, how KT–MT interactions remain dynamic throughout mitosis to enable chromosome movement and correction of attachment errors, which can result in genetic instability, remains incompletely understood (Godek et al., 2015; Heald and Khodjakov, 2015).

KT–MT attachment is predominantly mediated by the NDC80 complex that forms a dynamic and disordered MT-binding interface (Zaytsev et al., 2014). NDC80 is inhibited by Aurora-B-mediated multisite phosphorylation (DeLuca et al., 2011; Zaytsev et al., 2015), and a concept has emerged that shifting of the NDC80 MT-binding interface in and out of spatially separated zones dominated by either kinase or phosphatase activities underlies tension-induced hardening of KT–MT interactions (Liu et al., 2010; Welburn et al., 2010). Although the NDC80 complex is required for stable KT–MT attachment and force generation (DeLuca et al., 2005), other MT-binding activities localize to KTs (Godek et al., 2015), but the contribution of these proteins to KT–MT interactions remains unclear.

CLASPs are amongst the outermost KT proteins (Wan et al., 2009) that bind to CENP-E through their C-terminal domain (Maffini et al., 2009) and associate along MTs directly and to growing MT plus ends through interactions with EB1 (Mimori-Kiyosue et al., 2005; Wittmann and Waterman-Storer, 2005). CLASPs are required for mitosis (Maiato et al., 2003; Mimori-Kiyosue et al., 2006; Pereira et al., 2006) and may promote MT polymerization at the KT (Maiato et al., 2005; Young et al., 2014). The activity of CLASPs is controlled by phosphorylation predominantly in two intrinsically disordered regions. Phosphorylation by Cdk1 and Plk1 near to the KT-binding domain (Fig. 1A) contributes to normal chromosome dynamics and may stabilize KT–MT interactions, although the precise molecular mechanism remains elusive (Maia et al., 2012). In addition, we have previously identified multisite phosphorylation by Cdk1 and GSK3 (of which there are two isoforms encoded by *GSK3A* and *GSK3B*) near to the central SxIP EB1-binding motifs (where x indicates any amino acid) (Kumar et al., 2009). Although a mitotic role for GSK3 in chromosome segregation has been proposed (Tighe et al., 2007; Wakefield et al., 2003), no mitosis-specific GSK3 substrates have been identified. Here, we demonstrate that Cdk1 and GSK3-dependent phosphorylation control CLASP2 MT-binding throughout the cell cycle, and we report the effects of GSK3 phosphorylation-site mutants on KT and chromosome dynamics that are consistent with local KT-associated activation of CLASP–MT binding.

RESULTS

GSK3-mediated phosphorylation inhibits mitotic CLASP2α MT binding

Phosphorylation by Cdk1 and GSK3 strongly inhibits binding of an N-terminally truncated CLASP2 [comprising residues 497-1515; CLASP2(497-1515)] construct to MTs (Kumar et al., 2012). This raises a paradox of how CLASP2 can contribute to KT–MT interactions if the CLASP2 MT-binding activity is globally turned off during mitosis. CLASP2(497-1515) contains the EB1-binding SxIP motifs and a domain that we have identified as being required for direct CLASP2–MT binding (Fig. 1A) (Wittmann and Waterman-Storer, 2005). Recent X-ray crystallography confirms that this domain (TOG3) has a TOG-like fold that is characteristic for tubulin interactions (Maki et al., 2015). Indeed, mutation of positively charged residues in TOG3 surface loops specifically abolished binding along MTs without inhibiting plus-end tracking (Fig. 1C,D). This indicates that, in addition to SxIP-motif-mediated interactions with EB1 on growing MT ends, TOG3 contributes to

Department of Cell & Tissue Biology, University of California San Francisco, 513 Parnassus Avenue, San Francisco, CA 94143, USA.
*Present address: BioMarin Pharmaceutical Inc., San Rafael, CA, USA. ‡Present address: Gilead Biosciences Inc., 362 Lakeside Drive, Foster City, CA 94404, USA.

§Author for correspondence (torsten.wittmann@ucsf.edu)

T.W., 0000-0001-9134-691X

Received 6 July 2016; Accepted 20 February 2017

Journal of Cell Science (2017) 130, 1404-1412 doi:10.1242/jcs.194662

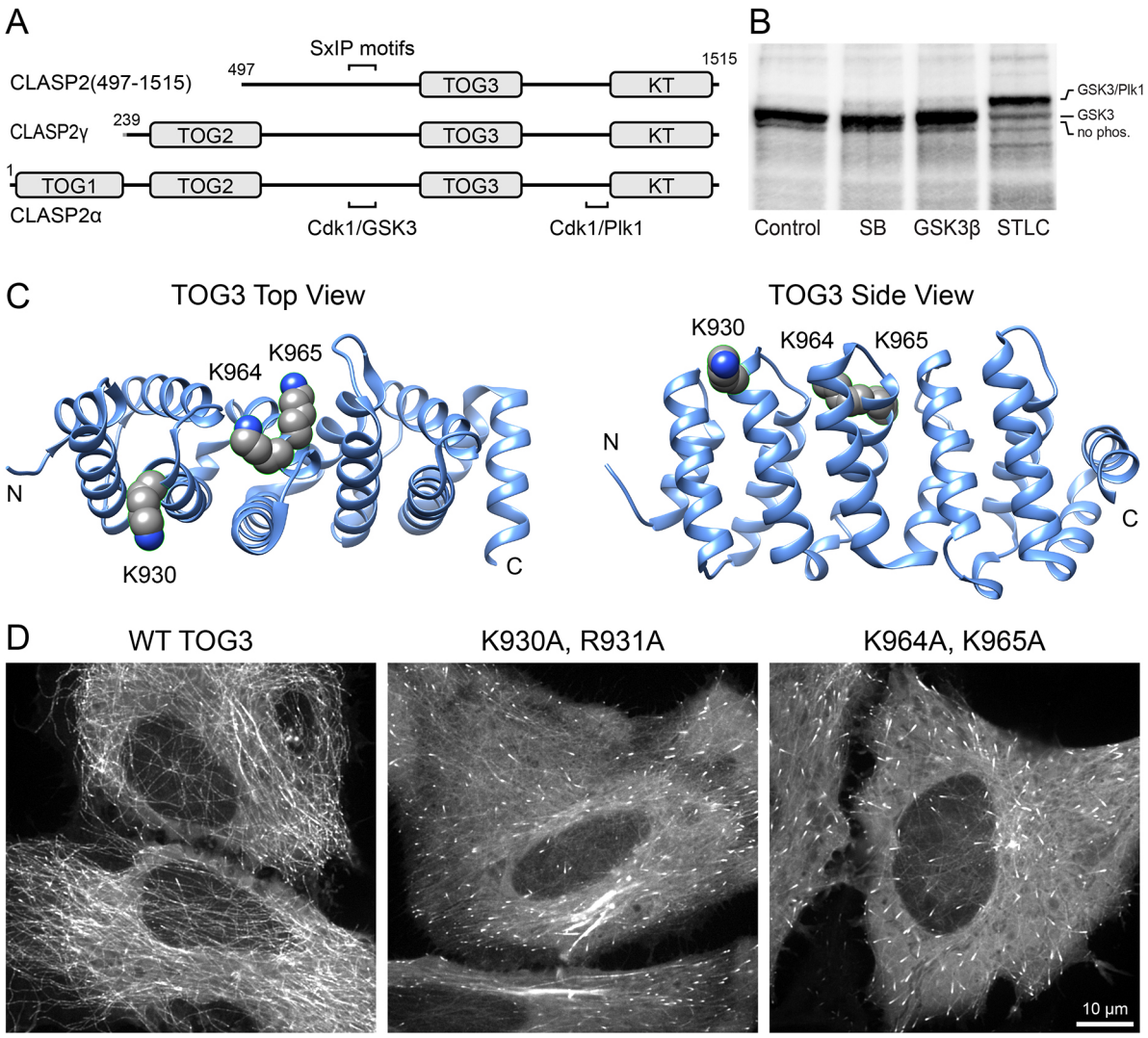

Fig. 1. Positively charged surface loops in TOG3 are necessary for CLASP2 binding along MTs. (A) Domain structure of human CLASP2 isoforms and truncated CLASP2(497-1515) depicting the three TOG domains, the KT-binding domain (KT) and intrinsically disordered multisite phosphorylation regions. NCBI reference sequences: CLASP2α NP_055912; CLASP2γ NP_001193973. (B) Immunoblot of endogenous CLASP2α in lysate from cells treated with a GSK3 inhibitor (20 µM SB216763), that expressed constitutively active GSK3β(S9A) (GSK3β) or that had been arrested in mitosis with an Eg5/KIF11 inhibitor (5 µM STLC). For full-length CLASP2α, the GSK3-mediated gel shift is difficult to discern, and the migration of the different phosphorylated species is indicated. The faint band slightly below CLASP2α is likely to be unspecific. (C) Structures of the TOG3 domain from mouse CLASP2 (PDB ID: 3WOZ), which is identical to the human protein except this structure is missing arginine 931, showing the location of surface lysine residues in loops 2 and 3. (D) Images of HeLa cells expressing the non-phosphorylatable CLASP2(9×S/A) variant of EGFP–CLASP2(497-1515), which binds strongly along the MT lattice with additional amino acid substitutions as indicated in the charged surface loops. Mutation of the positively charged residues in either loop abolished binding along MTs but had no effect on MT plus-end association. WT, wild type.

direct CLASP2–MT interactions in interphase cells. However, the full-length isoforms CLASP2γ and CLASP2α, generated by alternative splicing, contain additional N-terminal TOG domains (Fig. 1A), but how TOG1 and TOG2 in mammalian CLASP2 contribute to MT binding is unclear (Patel et al., 2012). Therefore, to test whether MT association of the longest CLASP2α isoform is cell cycle regulated, we measured EGFP–CLASP2α on MT ends as a function of cell cycle phases (Fig. 2A,C). Similar to truncated CLASP2(497-1515), EGFP–CLASP2α binding to MT ends decreased after nuclear envelope breakdown, was lowest in metaphase, and increased again during anaphase, probably as a result of Cdk1 inactivation. A raise above interphase levels during telophase further suggests an excess of phosphatase activity during exit from mitosis.

CLASP2 is phosphorylated in two intrinsically disordered regions: surrounding the SxIP EB1-interaction motifs and adjacent to the KT-binding domain (Fig. 1A). Compared with shorter CLASP2 constructs, the GSK3-mediated upshift of the ∼170 kDa endogenous full-length CLASP2α in gels is difficult to discern (Fig. 1B) (Kumar et al., 2009). In contrast, in metaphase-arrested cells, a larger upshift of CLASP2α in gels indicated substantial additional phosphorylation at other non-GSK3 sites during mitosis, as previously reported (Maia et al., 2012). Thus, to test whether mitotic CLASP2α MT-binding inhibition was due to GSK3 multisite phosphorylation at the previously identified sites, we compared the MT-end-association of non-phosphorylatable or phosphomimetic versions of full-length or truncated CLASP2 in metaphase-arrested cells (Fig. 2B,D). Non-phosphorylatable EGFP–CLASP2α(9×S/A) (comprising mutation of nine serine residues to alanine) was enriched several-fold on MT ends in metaphase. In contrast, the difference between wild-type and

Journal of Cell Science (2017) 130, 1404-1412 doi:10.1242/jcs.194662

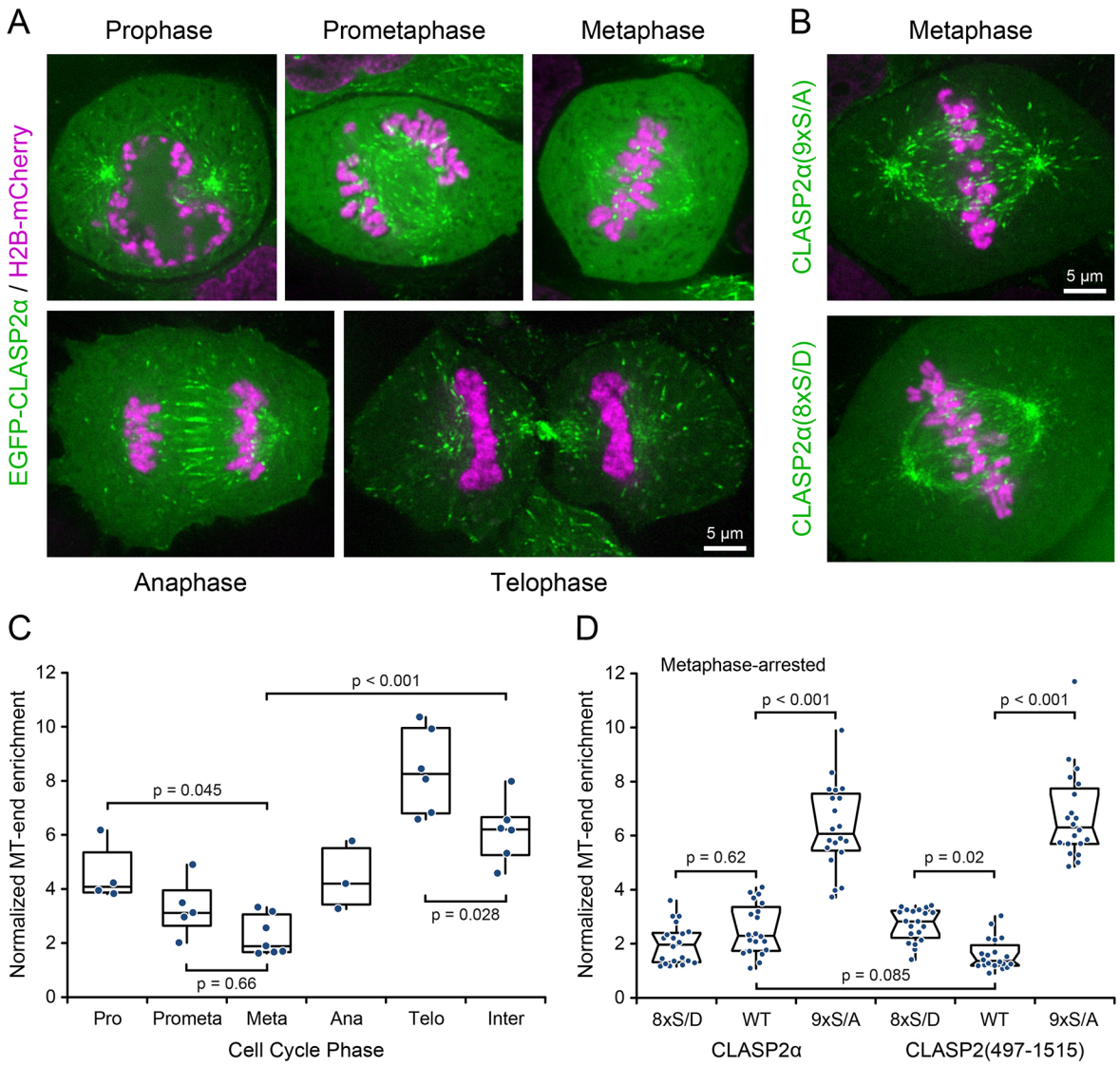

Fig. 2. Mitotic phosphorylation inhibits CLASP2α binding to MT ends. (A) EGFP–CLASP2α localization in different cell cycle phases in HaCaT cells that stably expressed histone-H2B–mCherry. (B) EGFP–CLASP2α phosphorylation-site mutants in cells arrested in metaphase with 10 µM MG132. (C) Analysis of EGFP–CLASP2α binding to growing MT ends during different phases of the cell cycle. (D) Comparison of binding to growing MT ends of the indicated CLASP2 phosphorylation-site mutations in metaphase-arrested spindles. Each dot represents the average of three measurements per cell. 8×S/D, eight serine phosphorylation sites mutated to aspartic acid residues in the CLASP2 constructs indicated; 9×S/A, nine serine phosphorylation sites mutated to alanine in the CLASP2 constructs indicated; Ana, anaphase; Inter, interphase; Meta, metaphase; Pro, prophase; Prometa, prometaphase; Telo, telophase; WT, wild type.

phosphomimetic EGFP–CLASP2α(8×S/D) (comprising mutation of eight serine residues to aspartic acid) was small and not significant. EGFP–CLASP2(497-1515) constructs behaved in a similar manner to full-length CLASP2α, except that wild-type EGFP–CLASP2(497-1515) showed slightly decreased MT binding, indicating that the N-terminal TOG domains only contribute to a small extent to CLASP2 binding to MT ends in mitotic cells. These data demonstrate that both direct and indirect MT interactions of all CLASP2 isoforms are greatly reduced in metaphase and are predominantly inhibited by GSK3-mediated phosphorylation in the central SxIP motif domain.

GSK3-mediated CLASP2α phosphorylation does not directly control KT binding

Because the KT-binding domain at the CLASP2 C-terminus is far from the central GSK3-phosphorylated region (Fig. 1A), we next tested whether GSK3 phosphorylation influences CLASP2 binding to KTs. Interestingly, compared with wild-type, non-phosphorylatable EGFP–CLASP2α(9×S/A) was enriched several-fold at KTs (Fig. 3A,B). However, nocodazole-induced MT depolymerization completely eliminated this enrichment. We therefore concluded that this increase reflects increased binding of EGFP–CLASP2α(9×S/A) to growing MT ends at KTs rather than direct KT binding itself.

Consistent with an enrichment at growing KT–MTs, EGFP–CLASP2α(9×S/A) fluorescence was often increased at one sister KT and not the other (Fig. 3A). During sister KT oscillations, only the KT moving away from the pole (anti-poleward) is expected to associate with polymerizing MT ends, and thus bind to increased amounts of +TIPs. To test if EGFP–CLASP2α(9×S/A) indeed identified polymerizing KT MTs, we analyzed time-lapse sequences of mitotic cells expressing EGFP–CLASP2α constructs

Journal of Cell Science (2017) 130, 1404-1412 doi:10.1242/jcs.194662

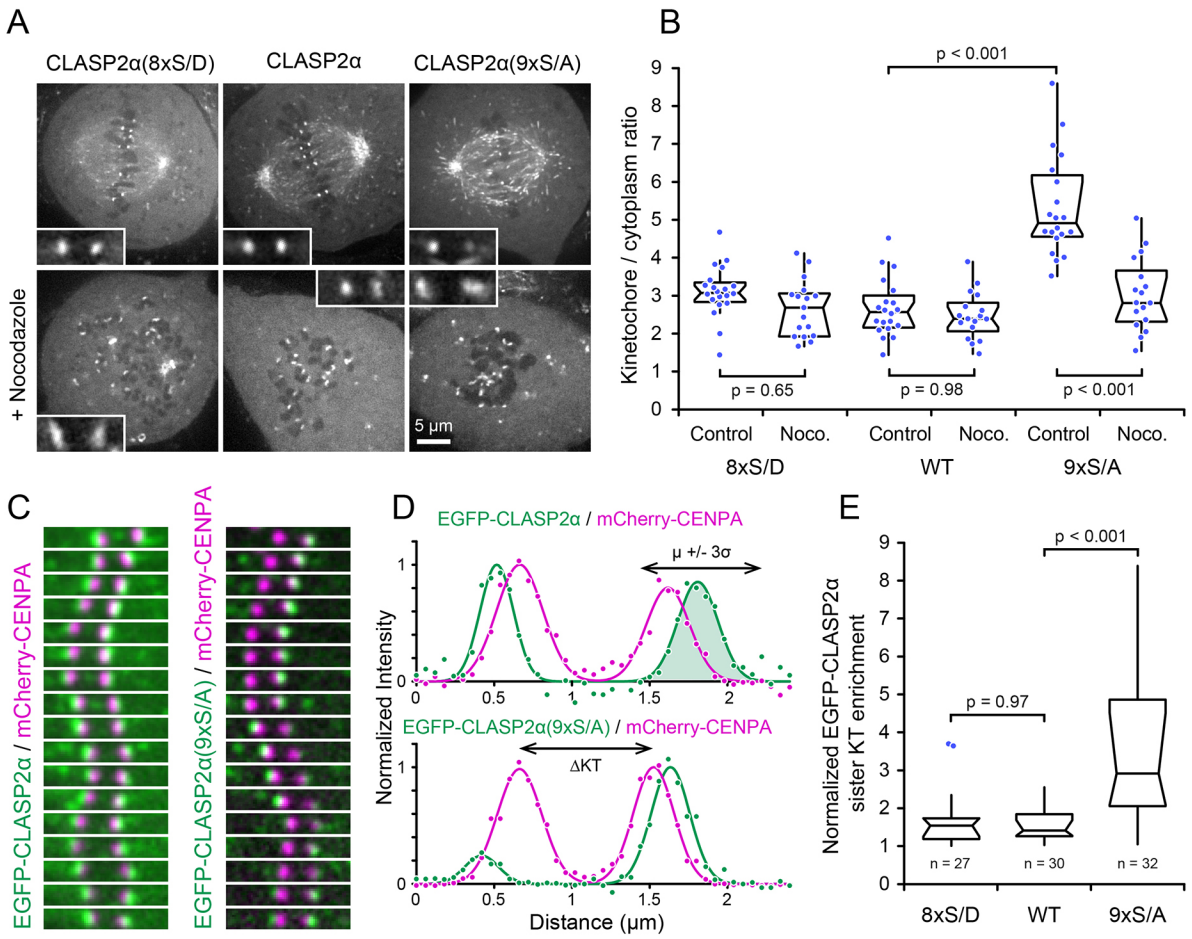

Fig. 3. CLASP2α binding to KTs is not directly controlled by GSK3-mediated phosphorylation. (A) Metaphase-arrested HaCaT cells expressing the indicated EGFP–CLASP2α phosphorylation-site mutants (top) and, in addition, treated with 1 µM nocodazole (bottom). Insets: KT pairs at higher magnification. (B) Relative enrichment of EGFP–CLASP2α on KTs compared to the signal in the cytoplasm. Each dot represents the average of three KT measurements per cell. Noco., nocodazole. (C) Time-lapse sequences of sister KT oscillations in metaphase cells expressing the indicated constructs illustrating EGFP–CLASP2α(9×S/A) (9×S/A) enrichment on the anti-poleward-moving sister KT. (D) Example intensity profiles across sister KT pairs showing double Gaussian fits (solid line) and illustrating how distances between sister KTs (ΔKT) and KT-associated fluorescence intensity was calculated. (E) The EGFP–CLASP2α fluorescence ratio between sister KTs. *n*=number of KT pairs analyzed. Outliers are shown as individual data points. 8×S/D, EGFP–CLASP2α(8×S/D); WT, wild type.

and mCherry–CENPA to mark KTs. Indeed, following the movements of individual KT pairs, EGFP–CLASP2α(9×S/A) was highly enriched at anti-poleward-moving KTs and switched to the opposite KT during direction reversal (Fig. 3C), indicating a high level of coordination of the MT polymerization state with KT movement. However, wild-type EGFP–CLASP2α did not appear to be enriched at the polymerizing KT MT bundle. We therefore quantified the relative enrichment of EGFP–CLASP2α by dividing the fluorescence intensity of the brighter KT by the dimmer one and normalizing to the mCherry–CENPA signal to correct for KT movements in and out of focus (Fig. 3D). As expected, this sister KT intensity ratio was high for EGFP–CLASP2α(9×S/A) (Fig. 3E). In contrast, the intensity ratio of KT-bound wild-type EGFP–CLASP2α or the phosphomimetic 8×S/D variant was close to one and not significantly different. This confirms that the amount of KT-bound CLASP2α is independent of the polymerization state of the KT–MT bundle (Pereira et al., 2006).

GSK3-mediated CLASP2 phosphorylation alters sister KT pair dynamics

In order to contribute to KT–MT interactions, we thus hypothesized that CLASP2α MT binding ought to be locally activated at KTs, presumably through local KT-associated dephosphorylation. Unfortunately, neither published (Watanabe et al., 2009) nor our own antibodies against the CLASP2 GSK3-phosphorylated motif S(p)QGCS(p)REAS(p) were sufficiently specific to visualize the local CLASP2 phosphorylation state by immunofluorescence. Instead, we tested the ensuing prediction that phosphorylation-deficient CLASP2α mutants act as dominant negatives by occupying KT binding sites and disrupting local control of CLASP2 binding to MTs at the KT.

As a readout for tension between KTs and a proxy for the strength of KT–MT interactions (Waters et al., 1996), we measured the distance between mCherry–CENPA-labeled sister KTs (ΔKT; Fig. 3D) at sub-resolution accuracy in cells expressing EGFP–CLASP2α phosphorylation-site mutants. In control cells, the average ΔKT was 1.13±0.14 µm (mean±s.d.) (Fig. 4A). Pharmacological inhibition of MT dynamics led to an expected relaxation of tension across KT pairs and a resulting ∼25–30% ΔKT decrease (nocodazole, 0.86±0.09 µm; taxol, 0.79±0.1 µm) (Magidson et al., 2016; Maresca and Salmon, 2009). Cells expressing wild-type EGFP–CLASP2α were indistinguishable from controls (1.13±0.14 µm). In contrast, in cells expressing the phosphomimetic 8×S/D variant, ΔKT was significantly reduced

Journal of Cell Science (2017) 130, 1404-1412 doi:10.1242/jcs.194662

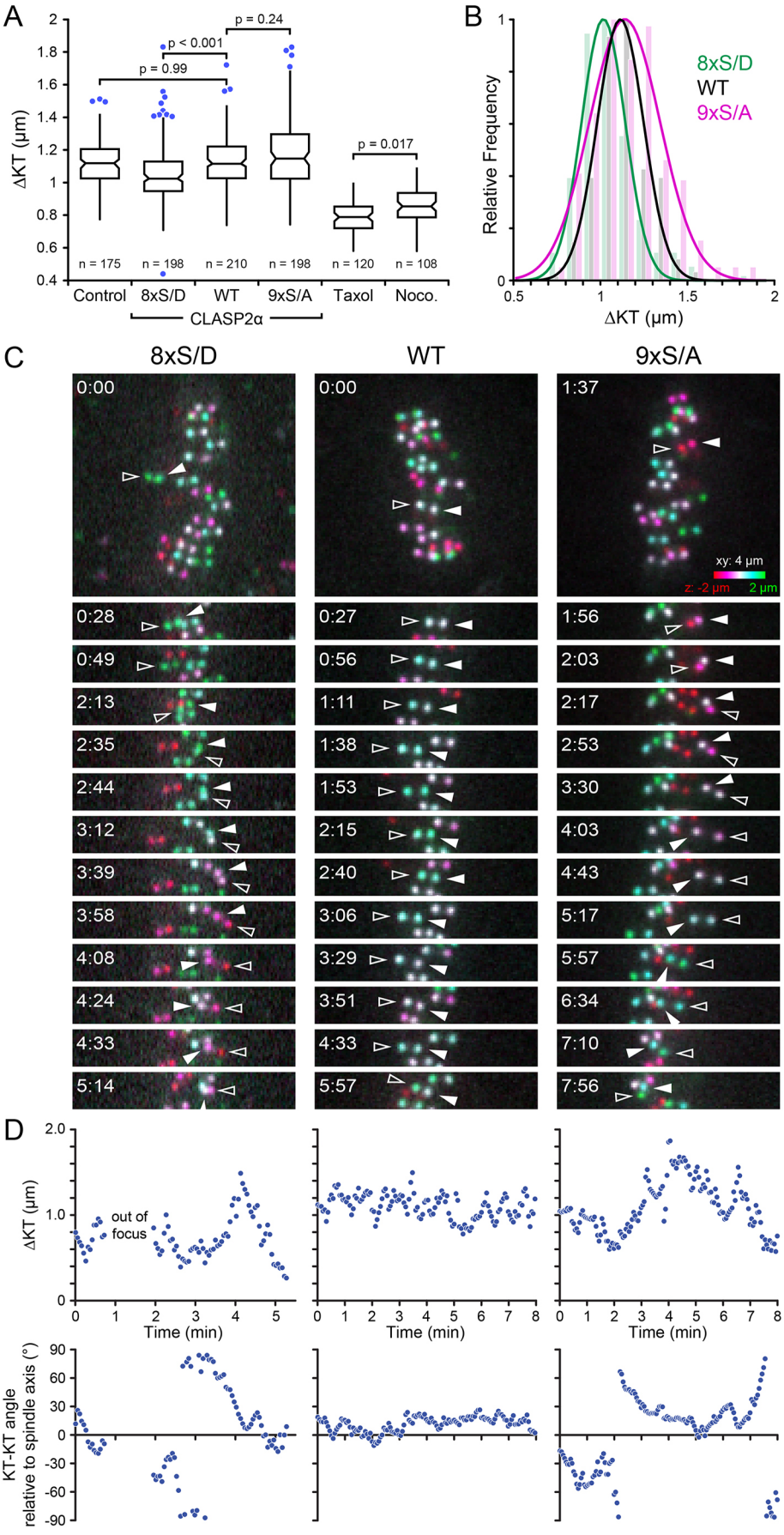

Fig. 4. GSK3-mediated CLASP phosphorylation weakens KT–MT interactions. (A) Analysis of ΔKT in cells expressing the indicated EGFP–CLASP2α constructs, or treated with 80 nM nocodazole (Noco.) or 1 μM taxol. *n*=number of KT pairs analyzed. Outliers are shown as individual data points. (B) ΔKT distributions plotted as histograms and overlaid with Gaussian fits (solid lines) illustrating differences in distribution means and widths. (C) Representative time-lapse data of CENPA–mCherry-labeled metaphase KT dynamics in cells expressing the indicated EGFP–CLASP2α constructs. Shown are color-coded maximum intensity projections to follow KT pairs over time (min:s). Solid and open arrowheads indicate sister KTs of specific pairs showing unusual dynamics in the cells expressing EGFP–CLASP2α phosphorylation-site mutants. (D) ΔKT and alignment relative to the spindle axis over time of the KT pairs indicated in C. 8×S/D, EGFP–CLASP2α (8×S/D); 9×S/A, EGFP–CLASP2α(9×S/A); WT, wild type.

Journal of Cell Science (2017) 130, 1404-1412 doi:10.1242/jcs.194662

by ∼10% to 1.05±0.17 µm. This is similar to the ΔKT decrease in CLASP1 CLASP2 double-knockdown cells (Mimori-Kiyosue et al., 2006) and consistent with the idea that non-phosphorylated CLASP2 partially contributes to KT–MT interactions and resulting tension across the KT pair. In contrast, a subtle increase in ΔKT in EGFP–CLASP2α(9×S/A)-expressing cells (1.17±0.21 µm) was not statistically significant. However, the distribution of ΔKT values in EGFP–CLASP2α(9×S/A)-expressing cells was skewed toward larger values (Fig. 4B), and the variance of the EGFP–CLASP2α (9×S/A) population was statistically significantly increased compared with that of wild type (P<0.0001, Brown–Forsythe test), unlike the variance of the EGFP–CLASP2α(8×S/D) population, which was not different (P=0.28). Taken together, these data indicate that although CLASP2α in the cytoplasm is hyperphosphorylated during metaphase, a population of KT-bound CLASP2α is likely to be locally dephosphorylated and contributes measurably to KT–KT tension. These findings are also consistent with a GSK3-inhibitor-induced ΔKT increase (Tighe et al., 2007) and suggest that CLASP2 is an important KT-associated GSK3 substrate. In addition, the large outlier ΔKT values in cells that expressed the non-phosphorylatable mutant suggest that there are instances at which KT-bound CLASP2 binding to MTs must be reduced as part of normal metaphase KT dynamics.

To test how the CLASP2 phosphorylation state influences KT dynamics, we analyzed time-lapse sequences of metaphase cells expressing mCherry–CENPA. In control cells, KT pairs oscillated back and forth while retaining a roughly perpendicular orientation to the metaphase plate, indicating a balanced attachment of the sister KTs to either spindle pole (Fig. 4C). However, in cells expressing CLASP2α phosphorylation-site mutants, we occasionally observed highly unusual KT dynamics. In EGFP–CLASP2α(8×S/D) cells, KT pairs sometimes drifted out of the metaphase plate, accompanied by a substantial decrease in ΔKT and a loss of perpendicular orientation relative to the metaphase plate, consistent with temporary loss of MT attachment to one of the sister KTs (Fig. 4C,D). In contrast, in EGFP–CLASP2α(9×S/A) cells, KT pairs sometimes appeared to be pulled out of the metaphase plate, stretching KT pairs to generate almost twice the average ΔKT in control cells (Fig. 4C,D). This is consistent with our prediction that CLASP2 phosphorylation by GSK3 reduces KT–MT interactions. In ∼25 cells examined per condition, we estimate a ∼threefold increase in these abnormal KT dynamics compared with controls. However, these events were too infrequent to unambiguously establish that these correlated with the expression of CLASP2α phosphorylation-site mutants, and we were unable to reliably detect such anomalous KT behavior by computer-assisted tracking of the entire KT population (Jaqaman et al., 2010). Even if these unusual KT dynamics are not correlated with CLASP2 MT-binding activity, it is important to note that such non-standard KT behavior occurs in metaphase cells.

Because even small errors in KT–MT attachment can result in chromosome segregation defects and aneuploidy (Thompson and Compton, 2011), we tested how expression of EGFP–CLASP2α phosphorylation-site mutants affect mitotic fidelity. To increase the percentage of cells in anaphase, we released cells from a G2–M block, and fixed and counted cells that exhibited lagging chromosomes in anaphase or chromosome bridges in telophase (Fig. 5A). Expression of either phosphorylation-site mutant notably

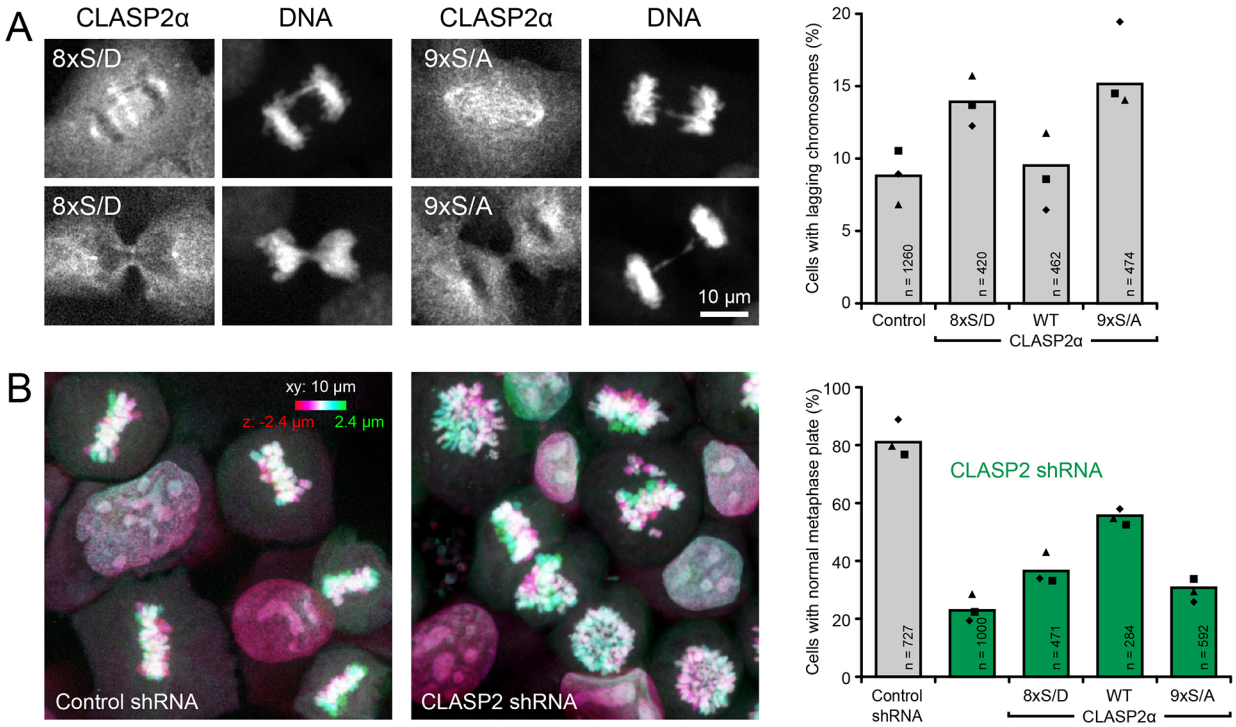

Fig. 5. Dynamic CLASP2 phosphoregulation promotes error-free chromosome segregation. (A) Representative images of anaphase and telophase cells expressing EGFP–CLASP2α GSK3 phosphorylation-site mutants with chromosome segregation defects. Bar graph shows the proportion of cells in or post anaphase with lagging chromosomes or chromatin bridges. (B) Mitotic forms in MG132-arrested control cells and cells in which CLASP2 had been depleted using shRNA. The graph shows the proportion of cells with normally aligned metaphase plates in cells in which the knockdown phenotype was rescued by expression of the indicated EGFP–CLASP2α phosphorylation-site mutants. In both A and B, different symbols show mean results from three independent experiments, and the bar graphs show the overall mean of these experiments. n=total number of mitotic cells analyzed. 8×S/D, EGFP–CLASP2α(8×S/D); 9×S/A, EGFP–CLASP2α (9×S/A); WT, wild type.

Journal of Cell Science

Journal of Cell Science (2017) 130, 1404-1412 doi:10.1242/jcs.194662

increased these segregation defects, while expression of wild-type EGFP–CLASP2α had no effect. Similarly, only wild-type EGFP–CLASP2α partially rescued mitotic phenotypes resulting from expression of shRNA against CLASP2, but phosphorylation site mutants did not (Fig. 5B).

DISCUSSION

In this paper, we examine the consequences of GSK3-mediated phosphorylation in the MT-binding domain of CLASP2 during mitosis. We show that the MT-binding activity of all CLASP2 isoforms is inhibited globally during metaphase, and we demonstrate the consequences of CLASP2 phosphorylation-site mutants on KT–KT tension and on the fidelity of chromosome segregation. However, neither the GSK3-mediated CLASP2 phosphorylation state nor the polymerization state of the KT–MT bundle appeared to affect CLASP2 localization to KTs. We find that only the non-phosphorylatable CLASP2α mutant was strongly enriched at growing KT MT bundles. This is similar to what has been observed for EB1 in Ptk1 cells (Tirnauer et al., 2002), and it is thus likely that this enrichment is due to increased binding to EB1. This is further consistent with the increased MT-end tracking of non-phosphorylatable CLASP2α during metaphase and indicates dephosphorylation of wild-type CLASP2α near to the KT. Of note, even though the KT area increased in nocodazole-treated cells, in contrast to previous reports (Pereira et al., 2006), we were unable to detect an increase of the amount of KT-bound EGFP–CLASP2α per unit area when MTs were depolymerized, which could be due to differences in methodology. We measured EGFP–CLASP2α fluorescence enrichment on KTs compared to the signal in the cytoplasm in live cells, and not by immunofluorescence in which a substantial amount of cytoplasmic EGFP–CLASP2α may be extracted during fixation. Unfortunately, our KT dynamics data rely on the expression of dominant-negative CLASP2α GSK3 phosphorylation-site mutants as we did not succeed in stably replacing endogenous CLASP2 activity. Possibly because of the presence of endogenous CLASP2, the overall effect on KT dynamics was small and, because it remains technically challenging to detect and quantify abnormal KT dynamics in mammalian cells, we were unable to unambiguously dissect how GSK3-mediated CLASP2 phosphorylation contributes to correct chromosome segregation. However, because the predominant MT-binding activity of KTs resides within the NDC80 complex, it is unsurprising that KT-dynamics defects resulting from disruption of CLASP2 phosphoregulation were subtle, and the precise mechanism by which GSK3-mediated regulation of CLASP2 MT-binding contributes to the robustness of error-free chromosome segregation remains to be determined.

Nevertheless, our data support a mitotic function of these GSK3 phosphorylation sites at KTs and further support a model in which GSK3-mediated phosphoregulation of CLASP2 interactions with MT plus ends contributes to the fine-tuning of the KT–MT interaction. We propose that CLASP2 is globally hyperphosphorylated during mitosis by GSK3 (Kumar et al., 2012), which inhibits its MT-binding activity. CLASP2-mediated KT–MT interactions therefore imply a local activation of CLASP2–MT binding that we believe could result from local dephosphorylation of GSK3 sites of only KT-bound CLASP2 molecules (Fig. 6). This proposed local activation of CLASP2–MT binding by KT-associated dephosphorylation is conceptually similar to the tension-regulated phosphorylation of the MT-binding state of the NDC80 complex (Welburn et al., 2010; Zaytsev et al., 2015). However, CLASP2 localization to the outer KT places it in the zone of proposed high phosphatase activity (Funabiki and Wynne, 2013) that is possibly independent of tension-mediated intra-KT structural rearrangements (Welburn et al., 2010). Although our data are consistent with this idea and we see very little CLASP2α localization to spindle MTs in metaphase, it should be noted that we cannot rule out other indirect effects of altered CLASP2–MT interactions. For example, stabilization of anti-parallel MT bundles could increase outward pushing forces and increase tension between sister KTs without directly altering KT–MT interactions (Liu et al., 2009). In addition to simply contributing to the KT–MT linkage, KT-bound active CLASP2 is also likely to promote polymerization of KT MTs (Funk et al., 2014; Maiato et al., 2005), which could indirectly alter KT-pair dynamics. Non-phosphorylatable CLASP2 could result in chromosome alignment defects by aberrantly pushing KT pairs out of the metaphase plate. Finally, how GSK3-mediated control of CLASP2–MT binding is integrated with Plk1-mediated CLASP2 phosphorylation that stabilizes and fine-tunes KT–MT attachment remains to be determined (Maia et al., 2012).

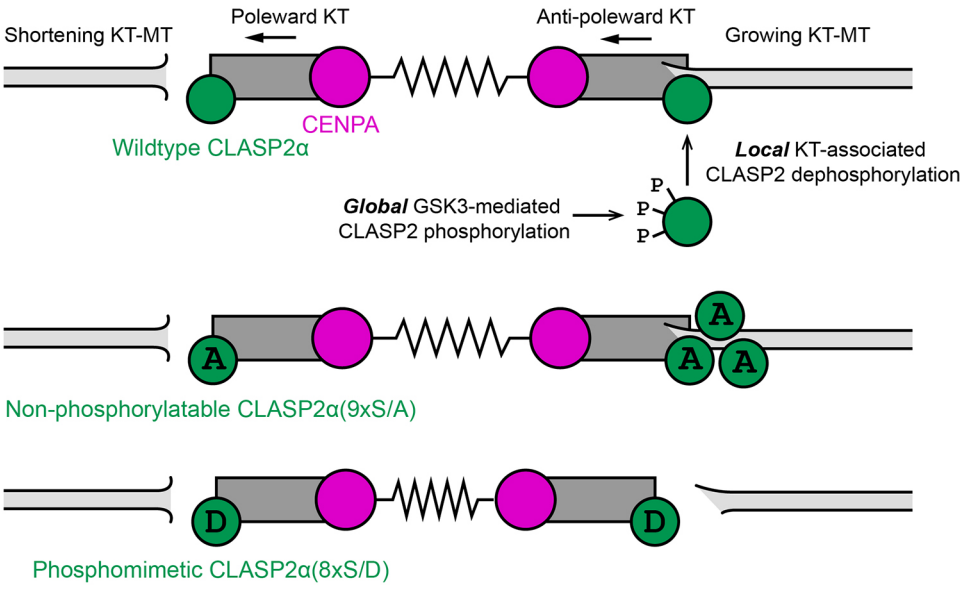

Fig. 6. Model of KT-associated CLASP2α phosphoregulation. We propose a hypothetical model in which CLASP2 at the KT is locally activated by dephosphorylation, which is consistent with the observed localization and changes in KT dynamics when CLASP2 GSK3 phosphorylation-site mutants are expressed.

Journal of Cell Science (2017) 130, 1404-1412 doi:10.1242/jcs.194662

MATERIALS AND METHODS

Adeno- and lentiviral constructs

H2B–mCherry or CENPA–mCherry pLenti6/V5-DEST (Invitrogen) vectors were generated by subcloning from Addgene plasmid #21044 or pEGFP–CENPA (from Alexey Khodjakov, Wadsworth Center, New York State Department of Health, Albany, NY). CLASP2α was subcloned from pEGFP-CLASP2α (from Irina Kaverina, Vanderbilt University Medical Center, Nashville, TN) into pAd/CMV/V5-DEST (Invitrogen). Wild-type and non-phosphorylatable 9×S/A CLASP2(497-1515) constructs have been described previously (Kumar et al., 2012). CLASP2(8×S/D) and mutated CLASP2α constructs were generated by swapping fragments from XbaI/BamH1 digests.

Cell culture

HaCaT cells were maintained, and lenti- and adenovirus particles produced and utilized as described previously (Stehbens et al., 2014). Cells were infected with lentiviral non-targeting shRNAs or shRNAs against CLASP2 and selected for 3 days with puromycin (Invitrogen) starting 48 h after infection. For immunoblotting, cells were lysed in a protease, kinase and phosphatase inhibitor buffer (Kumar et al., 2009). Rat anti-CLASP2 antibodies were from Absea Biotechnology Ltd. (KT68, 1:1000). Secondary horseradish peroxidase (HRP)-conjugated antibodies were from Jackson ImmunoResearch Laboratories. Cells were synchronized by incubation with 9 µM RO-3306 (EMD BioScience) for 16 h, washed three times with PBS, fixed in 4% paraformaldehyde after 90-120 min and stained with 500 nM propidium iodide (Invitrogen, P3566).

Microscopy and image analysis

Spinning disk confocal microscopy in sealed imaging chambers was as described previously (Ettinger and Wittmann, 2014; Stehbens et al., 2012). For fast KT dynamics, an iXon EMCCD camera (Andor) and increased disk speed (3500 rpm) were used to achieve sufficient frame rates for multiple *z*-slices.

For all fluorescence measurements of different fluorescently tagged CLASP2 constructs, cells were selected that fell within the same range of fluorescence intensity and thus expression levels. To quantify MT-bound EGFP–CLASP2, fluorescence intensity was measured in a 3-pixel-wide intensity profile perpendicular to and near the MT plus end. After subtraction of the camera offset, this was fitted with a Gaussian function and total intensity integrated around the mean±3 s.d., which encompasses 99.7% of the integrated area, and then normalized to the expression level by dividing by the local cytoplasm intensity defined as the *y*-offset of the fitted Gaussian function. Similarly, the sister KT ratio was calculated by fitting a 3-pixel-wide intensity profile with a double Gaussian function, dividing the integrated intensity of the brighter KT by the dimmer one, and normalized for the CENPA–mCherry ratio to correct for focus differences. The relative amount of KT-bound EGFP–CLASP2 was measured in a small region of interest on the KT (I_{KT}) and a local matching region in the cytoplasm (I_{Cyto}), as well as dark background outside the cell (I_{Dark}), and ratios were calculated as: $(I_{KT}-I_{Dark})/(I_{Cyto}-I_{Dark})$.

Statistical analysis used Excel (Microsoft) and the Analyse-it add-in (Analyse-it Software, Ltd). Box plots show median (lines), first and third quartile (boxes), observations within 1.5× the interquartile range (whiskers), outliers or all data points (dots), and 95% confidence intervals (notches). *P*-values were calculated using the Tukey–Kramer honest significant difference (HSD) test. Least square curve fitting was performed using the Solver function in Excel.

Acknowledgements

We thank Alexey Khodjakov and Irina Kaverina for gifts of reagents.

Author contributions

H.P. and T.W. designed experiments, analyzed and interpreted data and wrote the manuscript. H.P. performed the majority of experiments. P.K. performed experiments. J.v.H. contributed to data analysis and writing.

Competing interests

The authors declare no competing or financial interests.

Funding

This work was supported by National Institute of General Medical Sciences grant R01 GM079139 and National Institutes of Health grant S10 RR26758 to T.W., and an American Heart Association predoctoral fellowship 11PRE7590115 to H.P. Deposited in PMC for release after 12 months.

References

DeLuca, J. G., Dong, Y., Hergert, P., Strauss, J., Hickey, J. M., Salmon, E. D. and McEwen, B. F. (2005). Hec1 and nuf2 are core components of the kinetochore outer plate essential for organizing microtubule attachment sites. *Mol. Biol. Cell* **16**, 519-531.

DeLuca, K. F., Lens, S. M. A. and DeLuca, J. G. (2011). Temporal changes in Hec1 phosphorylation control kinetochore-microtubule attachment stability during mitosis. *J. Cell Sci.* **124**, 622-634.

Ettinger, A. and Wittmann, T. (2014). Fluorescence live cell imaging. *Methods Cell Biol.* **123**, 77-94.

Funabiki, H. and Wynne, D. J. (2013). Making an effective switch at the kinetochore by phosphorylation and dephosphorylation. *Chromosoma* **122**, 135-158.

Funk, C., Schmeiser, V., Ortiz, J. and Lechner, J. (2014). A TOGL domain specifically targets yeast CLASP to kinetochores to stabilize kinetochore microtubules. *J. Cell Biol.* **205**, 555-571.

Godek, K. M., Kabeche, L. and Compton, D. A. (2015). Regulation of kinetochore-microtubule attachments through homeostatic control during mitosis. *Nat. Rev. Mol. Cell Biol.* **16**, 57-64.

Heald, R. and Khodjakov, A. (2015). Thirty years of search and capture: the complex simplicity of mitotic spindle assembly. *J. Cell Biol.* **211**, 1103-1111.

Jaqaman, K., King, E. M., Amaro, A. C., Winter, J. R., Dorn, J. F., Elliott, H. L., Mchedlishvili, N., McClelland, S. E., Porter, I. M., Posch, M. et al. (2010). Kinetochore alignment within the metaphase plate is regulated by centromere stiffness and microtubule depolymerases. *J. Cell Biol.* **188**, 665-679.

Kumar, P., Lyle, K. S., Gierke, S., Matov, A., Danuser, G. and Wittmann, T. (2009). GSK3beta phosphorylation modulates CLASP-microtubule association and lamella microtubule attachment. *J. Cell Biol.* **184**, 895-908.

Kumar, P., Chimenti, M. S., Pemble, H., Schonichen, A., Thompson, O., Jacobson, M. P. and Wittmann, T. (2012). Multisite phosphorylation disrupts arginine-glutamate salt bridge networks required for binding of the cytoplasmic linker-associated protein 2 (CLASP2) to end-binding protein 1 (EB1). *J. Biol. Chem.* **287**, 17050-17064.

Liu, J., Wang, Z., Jiang, K., Zhang, L., Zhao, L., Hua, S., Yan, F., Yang, Y., Wang, D., Fu, C. et al. (2009). PRC1 cooperates with CLASP1 to organize central spindle plasticity in mitosis. *J. Biol. Chem.* **284**, 23059-23071.

Liu, D., Vleugel, M., Backer, C. B., Hori, T., Fukagawa, T., Cheeseman, I. M. and Lampson, M. A. (2010). Regulated targeting of protein phosphatase 1 to the outer kinetochore by KNL1 opposes Aurora B kinase. *J. Cell Biol.* **188**, 809-820.

Maffini, S., Maia, A. R. R., Manning, A. L., Maliga, Z., Pereira, A. L., Junqueira, M., Shevchenko, A., Hyman, A., Yates, J. R., III, Galjart, N. et al. (2009). Motor-independent targeting of CLASPs to kinetochores by CENP-E promotes microtubule turnover and poleward flux. *Curr. Biol.* **19**, 1566-1572.

Magidson, V., He, J., Ault, J. G., O'Connell, C. B., Yang, N., Tikhonenko, I., McEwen, B. F., Sui, H. and Khodjakov, A. (2016). Unattached kinetochores rather than intrakinetochore tension arrest mitosis in taxol-treated cells. *J. Cell Biol.* **212**, 307-319.

Maia, A. R. R., Garcia, Z., Kabeche, L., Barisic, M., Maffini, S., Macedo-Ribeiro, S., Cheeseman, I. M., Compton, D. A., Kaverina, I. and Maiato, H. (2012). Cdk1 and Plk1 mediate a CLASP2 phospho-switch that stabilizes kinetochore-microtubule attachments. *J. Cell Biol.* **199**, 285-301.

Maiato, H., Fairley, E. A. L., Rieder, C. L., Swedlow, J. R., Sunkel, C. E. and Earnshaw, W. C. (2003). Human CLASP1 is an outer kinetochore component that regulates spindle microtubule dynamics. *Cell* **113**, 891-904.

Maiato, H., Khodjakov, A. and Rieder, C. L. (2005). Drosophila CLASP is required for the incorporation of microtubule subunits into fluxing kinetochore fibres. *Nat. Cell Biol.* **7**, 42-47.

Maki, T., Grimaldi, A. D., Fuchigami, S., Kaverina, I. and Hayashi, I. (2015). CLASP2 has two distinct TOG domains that contribute differently to microtubule dynamics. *J. Mol. Biol.* **427**, 2379-2395.

Maresca, T. J. and Salmon, E. D. (2009). Intrakinetochore stretch is associated with changes in kinetochore phosphorylation and spindle assembly checkpoint activity. *J. Cell Biol.* **184**, 373-381.

Mimori-Kiyosue, Y., Grigoriev, I., Lansbergen, G., Sasaki, H., Matsui, C., Severin, F., Galjart, N., Grosveld, F., Vorobjev, I., Tsukita, S. et al. (2005). CLASP1 and CLASP2 bind to EB1 and regulate microtubule plus-end dynamics at the cell cortex. *J. Cell Biol.* **168**, 141-153.

Mimori-Kiyosue, Y., Grigoriev, I., Sasaki, H., Matsui, C., Akhmanova, A., Tsukita, S. and Vorobjev, I. (2006). Mammalian CLASPs are required for mitotic spindle organization and kinetochore alignment. *Genes Cells* **11**, 845-857.

Patel, K., Nogales, E. and Heald, R. (2012). Multiple domains of human CLASP contribute to microtubule dynamics and organization in vitro and in Xenopus egg extracts. *Cytoskeleton* **69**, 155-165.

Pereira, A. L., Pereira, A. J., Maia, A. R., Drabek, K., Sayas, C. L., Hergert, P. J., Lince-Faria, M., Matos, I., Duque, C., Stepanova, T. et al. (2006). Mammalian CLASP1 and CLASP2 cooperate to ensure mitotic fidelity by regulating spindle and kinetochore function. *Mol. Biol. Cell* **17**, 4526-4542.

Stehbens, S., Pemble, H., Murrow, L. and Wittmann, T. (2012). Imaging intracellular protein dynamics by spinning disk confocal microscopy. *Methods Enzymol.* **504**, 293-313.

Stehbens, S. J., Paszek, M., Pemble, H., Ettinger, A., Gierke, S. and Wittmann, T. (2014). CLASPs link focal-adhesion-associated microtubule capture to localized exocytosis and adhesion site turnover. *Nat. Cell Biol.* **16**, 558-573.

Thompson, S. L. and Compton, D. A. (2011). Chromosome missegregation in human cells arises through specific types of kinetochore-microtubule attachment errors. *Proc. Natl. Acad. Sci. USA* **108**, 17974-17978.

Tighe, A., Ray-Sinha, A., Staples, O. D. and Taylor, S. S. (2007). GSK-3 inhibitors induce chromosome instability. *BMC. Cell Biol.* **8**, 34.

Tirnauer, J. S., Canman, J. C., Salmon, E. D. and Mitchison, T. J. (2002). EB1 targets to kinetochores with attached, polymerizing microtubules. *Mol. Biol. Cell* **13**, 4308-4316.

Wakefield, J. G., Stephens, D. J. and Tavaré, J. M. (2003). A role for glycogen synthase kinase-3 in mitotic spindle dynamics and chromosome alignment. *J. Cell Sci.* **116**, 637-646.

Wan, X., O'Quinn, R. P., Pierce, H. L., Joglekar, A. P., Gall, W. E., DeLuca, J. G., Carroll, C. W., Liu, S.-T., Yen, T. J., McEwen, B. F. et al. (2009). Protein architecture of the human kinetochore microtubule attachment site. *Cell* **137**, 672-684.

Watanabe, T., Noritake, J., Kakeno, M., Matsui, T., Harada, T., Wang, S., Itoh, N., Sato, K., Matsuzawa, K., Iwamatsu, A. et al. (2009). Phosphorylation of CLASP2 by GSK-3beta regulates its interaction with IQGAP1, EB1 and microtubules. *J. Cell Sci.* **122**, 2969-2979.

Waters, J. C., Skibbens, R. V. and Salmon, E. D. (1996). Oscillating mitotic newt lung cell kinetochores are, on average, under tension and rarely push. *J. Cell Sci.* **109**, 2823-2831.

Welburn, J. P. I., Vleugel, M., Liu, D., Yates, J. R., III, Lampson, M. A., Fukagawa, T. and Cheeseman, I. M. (2010). Aurora B phosphorylates spatially distinct targets to differentially regulate the kinetochore-microtubule interface. *Mol. Cell* **38**, 383-392.

Wittmann, T. and Waterman-Storer, C. M. (2005). Spatial regulation of CLASP affinity for microtubules by Rac1 and GSK3beta in migrating epithelial cells. *J. Cell Biol.* **169**, 929-939.

Young, S., Besson, S. and Welburn, J. P. I. (2014). Length-dependent anisotropic scaling of spindle shape. *Biol. Open.* **3**, 1217-1223.

Zaytsev, A. V., Sundin, L. J. R., DeLuca, K. F., Grishchuk, E. L. and DeLuca, J. G. (2014). Accurate phosphoregulation of kinetochore-microtubule affinity requires unconstrained molecular interactions. *J. Cell Biol.* **206**, 45-59.

Zaytsev, A. V., Mick, J. E., Maslennikov, E., Nikashin, B., DeLuca, J. G. and Grishchuk, E. L. (2015). Multisite phosphorylation of the NDC80 complex gradually tunes its microtubule-binding affinity. *Mol. Biol. Cell* **26**, 1829-1844.